CONF-950793--12

UCRL-JC-121471
PREPRINT

Measurement of Wavefront Structure from Large Aperture Optical Components by Phase Shifting Interferometry

C. R. Wolfe, J. K. Lawson, M. Kellam
R. T. Maney, and A. Demiris

This paper was prepared for submittal to the
SPIE's International Symposium on Optical Science,
Engineering, and Instrumentation
San Diego, California
July 9–14, 1995

May 12, 1995

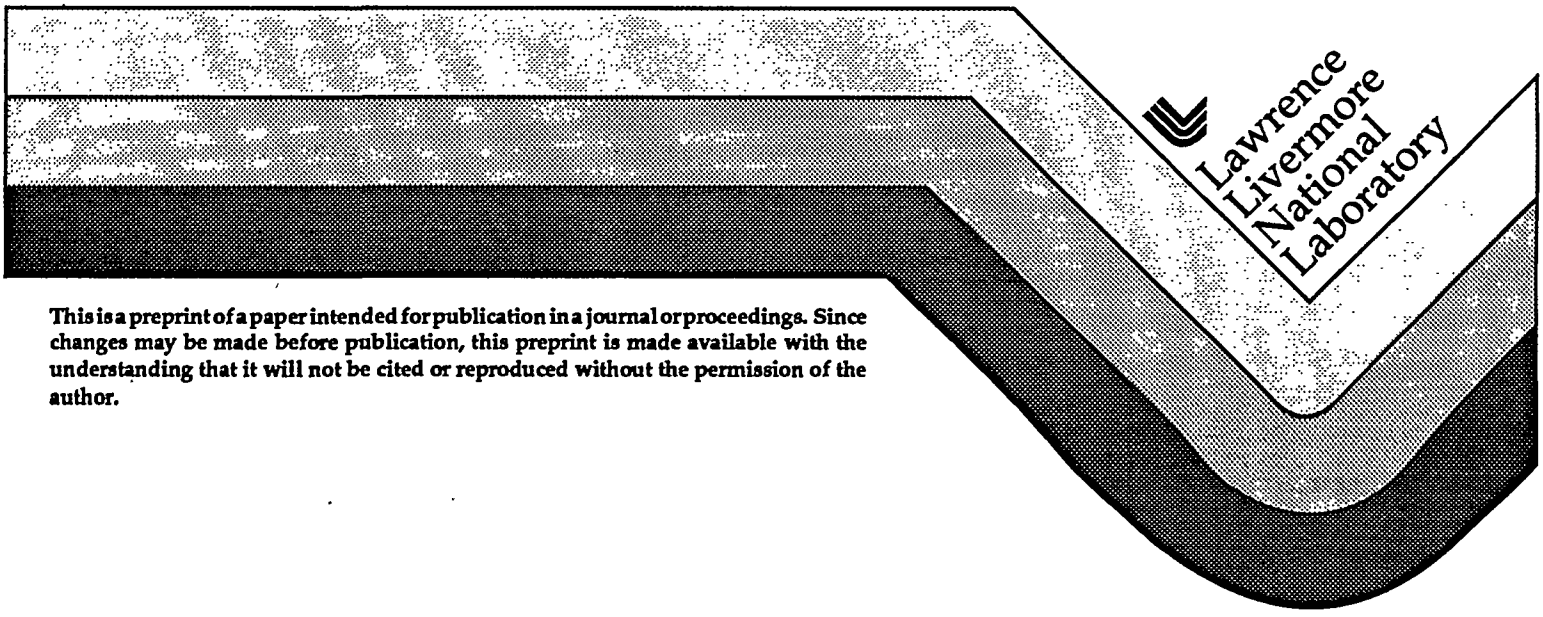

Measurement of wavefront structure from large aperture optical components by phase shifting interferometry

C. R. Wolfe, J. K. Lawson, M. Kellam, R. T. Maney and A. Demiris

Lawrence Livermore National Laboratory, L-487
P. O. Box 5508 Livermore, Ca., 94550

ABSTRACT

This paper discusses the results of high spatial resolution measurement of the transmitted or reflected wavefront of optical components using phase shifting interferometry with a wavelength of 6328 Å. The optical components studied range in size from approximately 50 mm x 100 mm to 400 mm x 750 mm. Wavefront data, in the form of 3-D phase maps, have been obtained for three regimes of scale length: "micro roughness", "mid-spatial scale", and "optical figure/curvature." Repetitive wavefront structure has been observed with scale lengths from 10 mm to 100 mm. The amplitude of this structure is typically $\lambda/100$ to $\lambda/20$. Previously unobserved structure has been detected in optical materials and on the surfaces of components. We are using this data to assist in optimizing laser system design, to qualify optical components and fabrication processes under study in our component development program.

Key words: Power Spectral Density, Fourier analysis, transmitted wavefront, reflected wavefront, phase shifting, Fizeau interferometer, wavefront modulation

1. INTRODUCTION

The performance of high-peak power laser systems such as the National Ignition Facility (NIF) can be seriously degraded by the presence of modulations in the beam. Beam modulations can be introduced or "imprinted" on the beam as it propagates by interaction with optical components. Examples include; transmissive components containing low amplitude variation in index of refraction and/or stress birefringence and optical surfaces containing low amplitude modulations. The sensitivity of the laser to beam modulation is determined by the subsequent growth (amplification) of these structures. This is dictated by the physics of non-linear optical gain and the geometry of spatial filtering employed for beam smoothing.

An early goal in our efforts to develop a cost optimized laser system design is to develop a realistic propagation model. This model must be able to predict beam behavior including the seeding of modulations and growth. The numerical calculations of the model [1] are based upon practical input parameters such as:

i. the accurate wavefront shape of optical components
ii. beam characteristics such as coherence, divergence, intensity and bandwidth,
iii. gain spectrum and
iv. the relevant non-linear optical physical principles.

Future lasers systems such as the NIF will require optical components with clear apertures on the order of 400 mm square. High spatial resolution measurement of the wavefront from parts of this size is now possible due to the highly developed instrumentation and techniques of phase shifting interferometry. The wavefront data that can now be obtained from proto-type parts will help establish the design basis of such lasers. This data will provide:

i. information about wavefront modulation for beam propagation modeling, laser system design and optimization,
ii. metrology data for optical component specification and
iii. a baseline of component wavefronts to assist in the development of advanced fabrication processes.

During the last decade the analysis capability and the spatial resolution of wavefront measurements from large apertures has greatly increased. Previously, only low resolution cameras were available and were used to detect phase information for scale lengths > 10 mm from static interferograms. This data was processed by fringe centering algorithms which digitized the static interferogram and interpolated the location of fringe centers. At best, several hundred data points were calculated. With only low frequency data, the wavefront was often constructed by fitting the data to Zernicke polynomials. This was the state of commercial instrumentation for wavefront analysis in the late '70s [2]. Today, the state of the art has changed greatly. High resolution solid state cameras, advanced phase shifting interferometry techniques and advanced computational algorithms are available to detect and calculate wavefront shape. Wavefront data can be obtained at each pixel of the high resolution solid state detector. Detectors with 640 x 480 or 740 x 480 pixels are common [3] in interferometry applications. Larger "mega-pixel" arrays, while not as common, are also available [4]. Equipped with high resolution detectors, modern interferometers are capable of exceeding 1 mm spatial resolution for test apertures of 400 x 400 mm size. Advanced phase shifting algorithms have, for the most part, replaced fringe centering algorithms. Modern algorithms that calculate the wavefront shape now routinely use data sets containing > 300,000 data points, rather than only points at interpolated fringe centers. Fourier analysis is replacing Zernicke polynomial fits, in many applications, when wavefront reconstruction is performed with high resolution data.

2. WAVEFRONT MEASUREMENT

2.1 Instrument description

The wavefront measurements that are reported here have been made at the Lawrence Livermore National Laboratory using three commercial instruments:

i. a 102 / 305 mm (4" / 12") aperture Zygo Mark IVxp® phase shifting Fizeau interferometer,
ii. a Maxim 3D® interference microscope equipped with Fizeau and Mirau type objectives. Both of these instruments are owned by the Materials & Measurement Engineering Division at LLNL, and
iii. a 102 / 457 mm (4" / 18") aperture Zygo GPIxp® phase shifting Fizeau interferometer, owned by the Laser Program at LLNL

The first two instruments are located in general purpose precision metrology laboratories with temperature control of approximately 68 ± 2.5 °F. The third instrument is located in a class 1000 cleanroom designed for fabrication of large aperture diffraction gratings, temperature control of that area is approximately 68 ± 1.0 °F. A sketch of the optical layout and photographs of the GPIxp Fizeau interferometer are shown in Figure 1. This instrument will be used extensively for metrology studies of large aperture ICF optical components in the future. It has the following capability:

i. two main test arms of 102 / 457 mm diameter aperture arranged in parallel, a turn mirror selects aperture to be used,
ii. a third, 33 mm diameter aperture, achieved by using a beam reduction telescope on the 102 mm arm,
iii. continuously variable magnification from 1 - 6x,
iv. a long coherence length, circular polarized light source with wavelength of 633 nm,
v. a solid state camera with 640 x 480 pixels (Sony commercial video),
vi. data transfer via "Ethernet" to / from other interferometers and computers used for wavefront analysis.

2.2 Bandwidth

The phase map shown in Figure 2 is a 38 mm square sub-aperture of the reflected wavefront from a diamond turned KDP crystal. It was measured with a 256 x 256 pixel camera. This aperture size was chosen to maximize the detection of wavefront features with scale lengths in the range from 1 to 10 mm. With an aperture of this size we can observe repetitive features with maximum lengths of approximately 1/3 of the aperture dimension (approximately 13 mm). The shortest scale length that can be observed is approximately 3x the ideal, Nyquist limited resolution. This lower limit is is approximately 0.9 mm. A modulation with spatial scale of 4 - 6 mm is clearly visible in Figure 2. This modulation is the result of a "wobble" of the lead screw

that controls the crystal translation when it is finished [5]. In contrast, the diamond tool feed marks, which have a scale length of approximately 4 μm, are not visible. These short scale length (high frequency) features lie outside the bandwidth of the measurement.

The bandwidth is determined by the composite optical transfer function (OTF) of the instrument [6]. The instrument transfer functions of interference microscopes and contact profilometers have been studied [7]. For an interferometer with a long coherence length source (the type used here) the transfer function is composed of contributions from the instrument optical system and the camera, or detector. Accurate wavefront characterization requires that the transfer function be measured or calculated, to determine instrument frequency response. Calculation of the OTF of commercial instruments is difficult because details concerning the optical designs are not available. However, the interferometer OTF(ν) can be determined by measuring the wavefronts from known phase objects and calculating the Fourier transform from the data. The OTF(ν) is the ratio of the measured Fourier amplitude spectrum to the ideal Fourier amplitude spectrum of the phase structure:

$$OTF(\nu) = A(\nu)_{measured} / A(\nu)_{calculated}$$

Raw wavefront data can be corrected or "restored" after the measurement by accounting for the instrument OTF(ν). This is done by multiplying the Fourier amplitudes, A(ν), in the spectrum, by 1 / OTF(ν) on a point-by-point basis and then taking the inverse transform. The "restored" wavefront will contain increased amplitudes for high frequency features compared to the raw data.

Raw wavefront data, uncorrected for actual bandwidth effects, can be used if comparative wavefront analysis is the object of the measurement. This is often the case when specifications include the test method and test instrument, or when monitoring a process for changes only. Measurements are in process to determine the OTF(ν) for the instruments as mentioned above: the phase maps shown below are raw data.

The spatial bandwidth can be extended by varying the interferometer aperture and/or the detector size (pixel count). This is illustrated in Figure 3, which shows how the "ideal" or detector limited bandwidth varies as interferometer aperture or detector pixel count is varied. In principle, wide bandwidth information can be obtained from multiple aperture measurements to yield data unobtainable from a single measurement [7]. If accurate wavefront data is required, the instrument OTF(ν) must be known at each aperture used.

2.3 Metrology requirements

The performance of high peak power laser systems can be seriously degraded by the presence of low amplitude periodic modulations in the surface and transmitted wavefronts of the optical components used. At high peak power, these phase modulations can convert into intensity modulations by non-linear optical processes [9, 10]. This in turn can lead to loss in energy on target via many well known mechanisms. In some extreme cases damage to optical components downstream of the source of the modulation can occur. The NIF baseline design [11, 12] requires 192 beamlines containing many large optical elements such as laser slabs, KDP crystals, mirrors, polarizers, lenses and windows. In all, approximately 7,000 large aperture optical components are required. The wavefront requirements of optical components in the NIF depend on their location and function; i.e. whether an element is transmissive or reflective, the fluence incident on the part and whether the element encounters the first or third harmonic beam. The physics of the design further dictate three regimes of spatial scale length that are important for characterizing beam modulation. These regimes are:

i. short scale, or" micro roughness" having scale lengths < 0.12 mm,
ii. mid-spatial scale, with scale lengths from 0.12 to 33 mm and
iii. long scale, corresponding to optical figure / curvature having scale lengths > 33 mm.

Figure 4 is a matrix used to guide and summarize the status of our metrology effort. Listed in the left-hand column are the major optical components; across the top are three scale length regimes. Entries in the matrix indicate the predominant loss mechanism or threat to laser system performance. The priority associated with the need for the data for modeling purposes is also indicated. Shaded entries indicate areas were measurements have been made. As part of development of optical components for the NIF, we will measure proto-type parts as they become available. A database of wavefronts from these parts has been established for the purpose of laser system modeling [13].

2.4 Transmitted wavefront measurements

A primary use of the data described here is beam propagation modeling, therefore care is taken to measure transmissive parts at use angle. When the transmitted wavefront is measured in this orientation, the transmitted wavefront for the part is calculated by subtracting the wavefront of the empty cavity. Examples of the transmitted wavefront observed are shown in Figure 5a, b and c. These phase maps were measured with 38 mm square test apertures, to maximize the detection of features with 1 - 10 mm scale length. Figure 5a is a relatively smooth wavefront, while Figures 5b and c illustrate two forms of modulation that are sometimes observed. That data is reported as single-pass transmitted wavefront.

Full aperture measurement of NIF proto-type lenses is not possible in the Fizeau configuration due to their long focal length. The central on-axis portion of the wavefront can be measured,

however. An example of modulation detected in the transmitted wavefront of an f/15 aspheric spatial filter lens is shown in Figure 6. Full aperture measurement of the transmitted wavefront is generally be made using unequal path laser interferometer (LUPI). Such measurements are made by the lens fabricators.

2.5 Reflected wavefront measurements

Reflected wavefronts are generally measured at near normal incidence for conivance. When used for modeling purposes the reflected wavefronts must be corrected to the use angle condition. The reflected wavefront from transmissive components is not of direct interest to us for propagation modeling. For these components, surface structure is primarily important as it affects the transmitted wavefront. The ability to separate bulk and surface effects is important however when the fabrication process is under study. Once again, due to the large aperture and long focal length of proto-type lenses, only a sub-aperture can be measured in a Fizeau interferometer. Any sub-aperture can be measured, not just on-axis, but anywhere on the surface by tipping the lens about the optical axis. To detect very short scale length surface features, an interference microscope must be used. Very short scale length features on the surfaces of a spatial filter lens are shown in Figure 7.

3. WAVEFRONT ANALYSIS

3.1 Calculation of phase

Modern phase shifting interferometry is highly evolved. The optical technique of phase shifting traces its roots to work in the '60s, an early summary was written by Crane [14]. Data analysis is discussed more recently, in a review of algorithms by Creath [15]. Commercial Fizeau interferometers are available with apertures as large as 457 mm (18"). Custom instruments with slightly large aperture are probably possible [16]. Two methods are used to calculate the phase of the wavefront: the "phase stepping" and the "phase ramping" (aka: "integrating bucket") methods. The specific method and algorithm by which the phase is determined is generally a proprietary attribute of commercial instruments. However, the approaches can be easily explained for the "4 step algorithm". The intensity at each pixel of the detector has the form:

$$I_{pixel} = a + b\cos(\Theta)$$

where "a" is a constant, "b" is the fringe contrast or visibility and Θ is the phase. The phase at each pixel is measured four times. Phase increments of $\pi/2$ separate each measurement:

$I_1 = a + b\cos(\Theta)$,
$I_2 = a + b\cos(\Theta + \pi/2) = a - b\sin(\Theta)$,
$I_3 = a + b\cos(\Theta + \pi) = a - b\cos(\Theta)$ and

$I_4 = a + b\cos(\Theta + 3\pi/2) = a + b\sin(\Theta)$.

Then the phase at each pixel is:

$\Theta = \arctan \left[(I_4 - I_2) / (I_1 - I_3) \right]$.

The "integrating bucket" method is most often implemented because a settling time inherent in the "phase stepping" method is eliminated. In addition, the number of "buckets" of phase data collected isn't usually four, but another number optimized to enhance signal-to-noise for specific instrument and environmental conditions. Once the phase at each pixel is calculated, phase ambiguities are removed and the wavefront is constructed by connecting data points. For reliable removal of discontinuities, the phase must not change by $> \lambda/2$ between adjacent pixels. This requirement determines the maximum vertical step height and the maximum slope that can be resolved by the phase shifting technique.

After the wavefront has been constructed, the "shape" can be analyzed by various methods. This can include curve fitting and filtering so that specific wavefront attributes (shapes or spatial components) can be observed.

3.2 Data analysis by Fourier techniques

In the past wavefronts of ICF optical components have been described over a specific aperture in terms of P-V, gradient and rms. The performance of high peak power laser systems, such as the NIF, is dominated by diffraction and non-linear optical effects caused by the interaction of the collimated, high intensity, coherent and narrow bandwidth beam with materials and interfaces which can impart periodic modulation onto the propagating wavefront. These effects dictate three regimes of scale length as discussed in "Metrology requirements."

Traditionally, wavefront shape has been expressing by fitting the wavefront in terms of Zernicke polynomials [17]. Zernicke polynomials correctly describe only circular apertures, since the polynomials form an orthogonal set only for this aperture shape. Furthermore, Zernicke analysis treats only low spatial frequency wavefront aberrations commonly referred to as "shape" or "curvature"; the classical third order (Seidel) aberrations are calculated from the first eight polynomials. Mid-spatial scale and high frequency error are expressed only as "residuals" of the polynomial fit. Zernicke analysis can not take advantage of high resolution wavefront data because there are a limited number of polynomials (37) to fit, as it is commonly employed. The residual of the Zernicke fit can not be reduced below that calculated based on the "complete" or 37 term fit. These severe limitations on the use of Zernicke analysis suggests that an alternative method be used.

Fourier analysis of the high spatial resolution wavefront data produced by modern interferometers is appropriate to ICF modeling needs. It is potentially a very powerful method. There is no implicit limitation on either the aperture shape or the spatial resolution. Fourier wavefront analysis is limited only by the spatial bandwidth of the data available.

3.3 Physical interpretation of the Power Spectral Density

The Power Spectral Density (PSD) is calculated from the amplitude of frequency components in the wavefront Fourier amplitude spectrum. The PSD is a physically significant figure-of-merit for expressing the wavefront structure or shape. The PSD directly yields information about:

i. periodic wavefront structure through the appearance of peaks in the PSD,
ii. the average squared roughness $(RMS)^2$ of the wavefront for any frequency band for which data is available, and
iii. the intensity and distribution of scattered light.

The PSD is widely used by workers in the precision metrology field. Calculation of this function is straight-forward in principle [20] however care must be exercised when using commercial analysis software. The optical PSD, was developed during the '70s by those working to quantify optical scatter [21] and relate it to surface roughness of optical surfaces. The optical PSD was first formulated by Church [22, 23] and later proposed by Janeczko [24] to specify surface roughness of infrared materials. In 1-D, the magnitude of the PSD for a given frequency, ν_i, is calculated from the Fourier amplitude spectrum:

$PSD(\nu_i) = A(\nu_i)^2 / (\Delta\nu)$, and $\Delta\nu$ is the frequency increment.

where $A(\nu_i)$ is the Fourier amplitude for frequency ν_i.

If repetitive modulation is present in the wavefront, peaks will appear when the PSD is displayed vs. frequency (see Figures 8 - 11). These peaks correspond to large Fourier components at the frequency of the wavefront modulation. The integral of the PSD over a frequency range yields the RMS roughness of the wavefront. When the Fourier pair consist of distance (or scale length) and spatial frequency; Parseval's theorem [25] for Fourier series becomes a statement of the RMS surface roughness:

$$\int_{\nu_0}^{\nu} A(\nu_i)^2 \, d\nu = \sum_i c_i^2 .$$

Then:

$$\int_{\nu_0}^{\nu} PSD(\nu_i) \, d\nu = (RMS)^2 .$$

The RMS is valid over the same frequency interval as the PSD.

Further significance of the PSD comes from the physics of small angle scattering [26]. Fourier analysis reconstructs the measured wavefront by calculating an equivalent series of sinusoidal terms, each with amplitude A(v). The effect of such a surface on a propagating beam is to cause diffraction from the sinusoidal components. The direction of the diffracted light will be given by the grating equation. If the amplitude of the gratings, A(v), is much less than the wavelength of the light (as for NIF optics), then the intensity in each diffracted order is:

scattered intensity ~ (grating amplitude) ^{2}.

So the PSD is proportional to the scattered intensity and direction. The PSD can be used to calculate the intensity distribution in a propagating beam [27].

3.4 One dimensional Fourier analysis

A one dimensional PSD is sufficient to characterize a part if the wavefront structure is:

i. isotropic, then all directions are equivalent,
ii. "simple" (single frequency and unidirectional) and easy to observe (large magnitude) or
iii. only specified in one dimension or one direction on the part.

In these situations the direction of interest is specified by design or determined by the wavefront.

The Fourier analysis capability of the software that supports commercial instruments is limited. These analysis packages allow multiple profiles to be taken in the wavefront, but do not average them to reduce noise. Another potential concern are the assumptions made in the Fourier analysis, particularly when the profile selected does not contain a number of data point equal to an integer power of 2. In this case, the data often will be "padded" with zeros, often the analyst is not aware data "padding" can cause aliasing and erroneous frequencies in the Fourier spectrum. In order to better control the assumptions made in the Fourier analysis, we have developed our own software using a graphics based software package, Interactive Data Language (IDL®).

We have written a macro program that analyzes the wavefront data in the following steps, it

i. measures multiple (ten) profiles,
ii. calculates the PSD for each using a Hanning window on the profiles to suppress the effect of finite profile length,
iii. averages the PSDs and display the averaged result.

Examples of this capability applied to high spatial resolution wavefront data are shown in Figure 8 and 9. Signal averaging reduces the noise in the result by averaging multiple data sets to

calculate the 1-D PSD. Two phase maps measuring 38 mm square are shown in Figure 8a and 9a. A direction on the wavefront is chosen by selecting a "line-out" with a given physical length, L_0. The 1-D profiles are shown in Figures 8b and 9b. The data is then processed by a Fast Fourier Transform (FFT) routine. Raw PSDs for each profile are shown in Figures 8c and 9c. The averaged PSDs are shown in Figures 8d and 9d. The discrete Fourier transform [18, 19] defines the following characteristics in the amplitude spectrum :

$\nu_i = i/L_0$, where "i" is an integer and L_0 is the length of the "line-out" selected (including "padded zeros" if necessary)

ν_0, the lowest frequency, equal to $1/L_0$,

ν_{max}, the highest frequency, equal to (2x pixel or image resolution)$^{-1}$, also known as the Nyquist limit and

$\Delta\nu$, the increment between frequencies, ν_i, equal to $1/L_0$.

The units of PSD in 1-D are (length) ^{3}, in the examples used here: (Angstrom)^2 x (millimeter). The PSD is often expressed in log-log form to shown the wide range of amplitude variation in the Fourier spectrum.

3.5 Two dimensional Fourier analysis

Two dimensional Fourier analysis is necessary to fully characterize the wavefront if:

i. the wavefront is anisotropic,
ii. the structure in the wavefront isn't clearly visible (low magnitude) or if the shape of the structure is complex (more than one dominant frequency component or directions), or
iii. the part must be characterized in 2-D.

In general these are characteristics of wavefronts from NIF optical components. There is no preferred scattering direction about the propagation direction in the optical system, scattering and amplitude modulation is of concern equally in all directions. Therefore, wavefront modulations must be quantified uniformly in 2-D about the beam propagation direction.

Using IDL ® we have written software to calculate the PSD in 2-D. Analysis in 2-D makes use of the entire data set (> 300, 000 data points), this automatically accomplishes the signal averaging done by multiple "line-outs" in 1-D. Figures 10 and 11 show examples of 2-D Fourier analysis. Figures 10b and 11b show that data filtered with a Hanning window, a low frequency filter (cosine^2), used to prevent aliasing. Figure 10c and 11c display the calculated PSD, log scale. Finally, Figures 10d and 11d show a PSD surface, plotted on a linear scale. The wavefront modulation present in Figure 10a are primarily in 1-D. When this is the case, 2-D analysis adds little new information. In contrast, the wavefront shown in Figure 11a contains 2-D modulation

and 2-D analysis is necessary. The power of the 2-D analysis is apparent from this example, complex features over-looked by the simpler 1-D analysis are clearly resolved in 2-D. We intend to extend our work in 2-D analysis as part of the maturing beam modeling and propagation efforts in support of the NIF.

4. ACKNOWLEDGEMENTS

This work has been conducted in support of optical component development efforts in the ICF Program at the Lawrence Livermore National Laboratory. Specifically, during the last year we have revised specifications for optical components based, in part on the data and analysis described here. The authors express their gratitude to many individuals for assistance and insight concerning this work, including: D. M. Aikens, J. L. Atherton, J. M. Auerbach, R. E. English, J. T. Hunt, K. R. Manes and J. G. Vargas. This work was performed under auspices of the U S Department of Energy by the Lawrence Livermore National Laboratory under contract No. W-7405--ENG-48.

5. FIGURE TITLES / CAPTIONS

1a. Schematic drawing of the GPIxp interferometer layout
1b. The GPIxp 102/457 mm (4"/18") interferometer (photos)
2. A 38 mm square phase map of the reflected wavefront of crystal
LL-8-2: P-V = 0.086 λ, @ 633 nm
3 Ideal, or detector limited, frequency bandwidth vs. aperture diameter and detector element count.
4 Metrology matrix for NIF optical components
5 38 mm square aperture transmitted wavefronts from laser slab
5a. A relatively random, unmodulated wavefront,
P-V = 0.19 λ, @ 633 nm
5b. A wavefront exhibiting modulation primarily in 1-D, magnitude is l/70 with a scale lengths from 5 - 7 mm, P-V = 0.35 λ, @ 633 nm
5c. A wavefront exhibiting complex (curved, multiple frequencies) modulation, magnitude is l/100 with scale lengths from 5 - 7 mm,
P-V = 0.17 λ, @ 633 nm
6. Transmitted wavefront modulation detected in a spatial filter lens,
P-V = 0.037 λ ,@ 633 nm
7. Short scale length surface features detected on both the spherical and aspheric surfaces of a spatial lens
7a. Surface #1 aspheric, magnitude of modulation 9.1 nm,
over-all P-V = 35.5 nm
7b. Surface #2 spherical, magnitude of modulation 10.6 nm,
over-all P-V = 27.6 nm

8. An example of 1-D Fourier analysis of the reflected wavefront from a diamond turned KDP crystal surface (same data as Figure 2)
8a. Phase map with multiple profiles defined
8b. Profiles of phase height vs. position, taken from the map of Figure 8a
8c. Individual PSDs for each profile shown in Figure 8b
8d. The averaged PSD
9. Example of 1-D Fourier analysis of a transmitted wavefront
9a. Phase map with multiple profiles defined
9b. Profiles of phase height vs. position, taken from the map of Figure 9a
9c. Individual PSDs for each profile shown in Figure 9b
9d. The averaged PSD
10: Examples of 2-D Fourier analysis of a reflected wavefront (same data as Figures 2 and 8)
10a. Phase map data
10b. Phase map with Hanning window applied
10c. PSD calculated in 2-D
10d. PSD surface
11. Examples of 2-D Fourier analysis of a transmitted wavefront (same data file as Figure 9)
11a. Phase map data
11b. Phase map with Hanning window applied
11c. PSD calculated in 2-D
11d. PSD surface

6. REFERENCES

[1] J. M. Auerbach; *"Modeling beam propagation and frequency conversion for the Beamlet laser"*, ICF Quarterly Report Oct - Dec 1994, UCRL-LR-105821-95-1, p 80, published by UC Lawrence Livermore National Lab, available from: National Technical Information Service, US Department of Commerce, 5285 Port Royal Rd., Springfield Va., 22161

[2] W. Augustyn, et al; *"An automatic interference pattern processor with interactive capability"* Proc. of the SPIE vol. 153 p. 146 1978

[3] Wyko Corp., Phase Shift Technology , (both in Tucson Ariz.) and Zygo Corp. (Middlefield Conn.) sell instruments of this kind.

[4] There are several sources for "special" arrays, EG&G, Spectra Source and Dalsa are examples

[5] R. C. Montesanti; *"Fabrication of large Potassium di-Hydrogen Phosphate (KDP) crystals for the National Ignition Facility"*, SPIE Proc. of The First Annual International Conference: Solid State Lasers for Application to Inertial Confinement Fusion, May - June 1995, in press.

[6] E. L. Church et al; *"Direct comparison of mechanical and optical measurements of the finish of precision machined optical surfaces"*, Optical Engineering vol. 24 no. 3 p. 388 May/June 1985

[7] P. Z. Takacs; *"A step height standard for surface profile characterization"*, SPIE Proc. 1993, p 65
[8] E. L. Church, P. Z. Takacs; " Specification of glancing and normal incidence x-ray mirrors", Opt. Eng. v 34 no 2 p353, 1995
[9] V. I. Bespalov, V. I. Talanov; "Filamentary structure of light beams in non-linear liquids", JETP Lett. 3, p 307, 1966
[10] J. T. Hunt, D. R. Speck; *"Present and future performance of the Nova laser system"*, Opt. Eng. v 28, no 4, p 464, 1989
[11] National ignition facility conceptual design report, UCRL-PROP-117093, May 1994.
[12] Energy & Technology Review - December 1994: "The National Ignition Facility": UCRL-52000-94-12, published by UC Lawrence Livermore National Lab, available from: National Technical Information Service, US Department of Commerce, 5285 Port Royal Rd., Springfield Va., 22161
[13] C. R. Wolfe; "*A database of wavefront measurements for: laser system modeling, optical component development and fabrication process qualification*", SPIE Proc. this conference, in press
[14] R. Crane; *"Interference phase measurement"*, Applied Optics vol.8 no. 3 p. 538 March 1969
[15] K. Creath; *"Phase Measurement Interferometry Techniques"*, chapter V in Progress in Optics XXVI edited by E. Wolf: 1988 North-Holland Press Inc.
[16] Wyko, Zygo, Phase Shift Technology and others are considering large aperture commercial instruments.
[17] C-J. Kim, R. R. Shannon; *"Catalog of Zernicke Polynomials"*, chapter IV in Applied Optics and Optical Engineering - volume X edited by R. R. Shannon and J. C. Wyatt: Academic Press Inc. 1987
[18] M. R. Spiegel; *"Fourier Series and Applications"*, chapter 2 in Theory and Problems of Fourier Analysis : Schaums' Outline Series McGraw-Hill Inc., 1991
[19] R. D. Strum, D. E. Kirk; *"Discrete Fourier Transform"*, chapter 7 in Discrete Systems and Digital Signal Processing: Addison-Weslet Publishing Co., 1989
[20] J. M. Elson, J. M. Bennett; *"Calculation of the power spectral density from surface profile data"*, Applied Optics vol. 34 no. 1 p.201, January 1995
[21] J. M. Bennett and L. Mattsson; *"Scattering Theories and Surface Statistics"* , chapter 4 in Introduction to Surface Roughness and Scattering, published by, OSA: ISBN 1-55752-108-5, 1989
[22] E. L. Church et al; "*Direct comparison of mechanical and optical measurements of the finish of precision machined optical surfaces*", Optical Engineering May/June 1985, vol 24 no. 3
[23] E. L. Church; *"Fractal Surface Finish"*, Applied Optics 27, 1518, 1988
[24] D. J. Janeczko; *"Power Spectrum Standard for Surface Roughness: Part I"*, Proc. SPIE Vol. 1165 Scatter from Optical Components (1989) p 175
[25] J. D. Gaskill; Linear systems, Fourier transforms and optics, p. 217, John Wiley and Sons 1978.

[26] J. C. Stover; *"Introduction to light scatter"* chapter 1 in Optical Scattering Measurement and Analysis, see discussion of small angle approximation and references: McGraw-Hill Inc., Optical and Electro-optical Engineering Series, 1990, ISBN 0-07061814-3
[27] G. Gallatin; *"Wavefront Power Spectrum and Scattering"* unpublished, currently with SVG Lithography Wilton, Conn.

Top view:

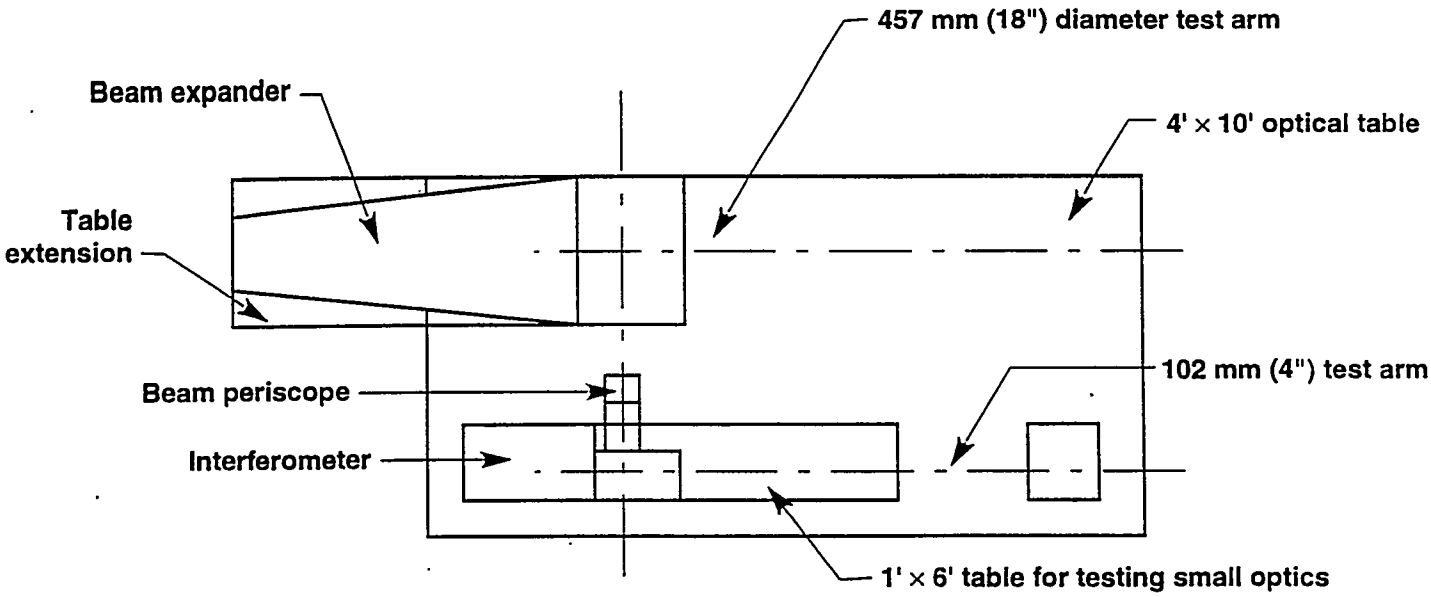

Elevation view:

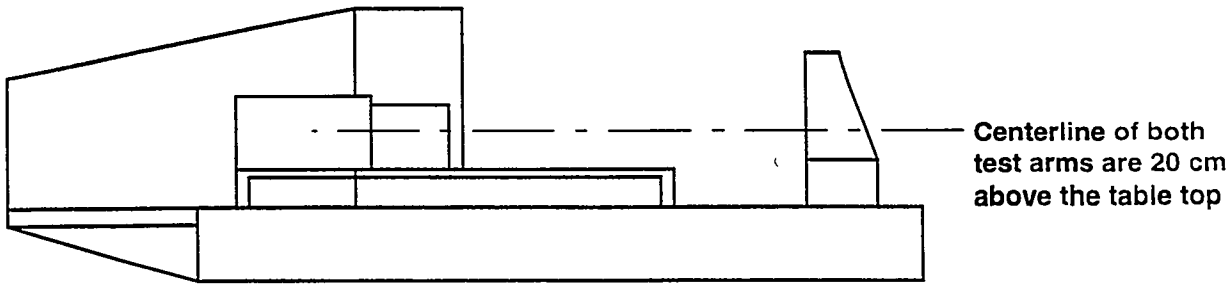

Figure 1a:
Schematic drawing of the GPIxp interferometer layout

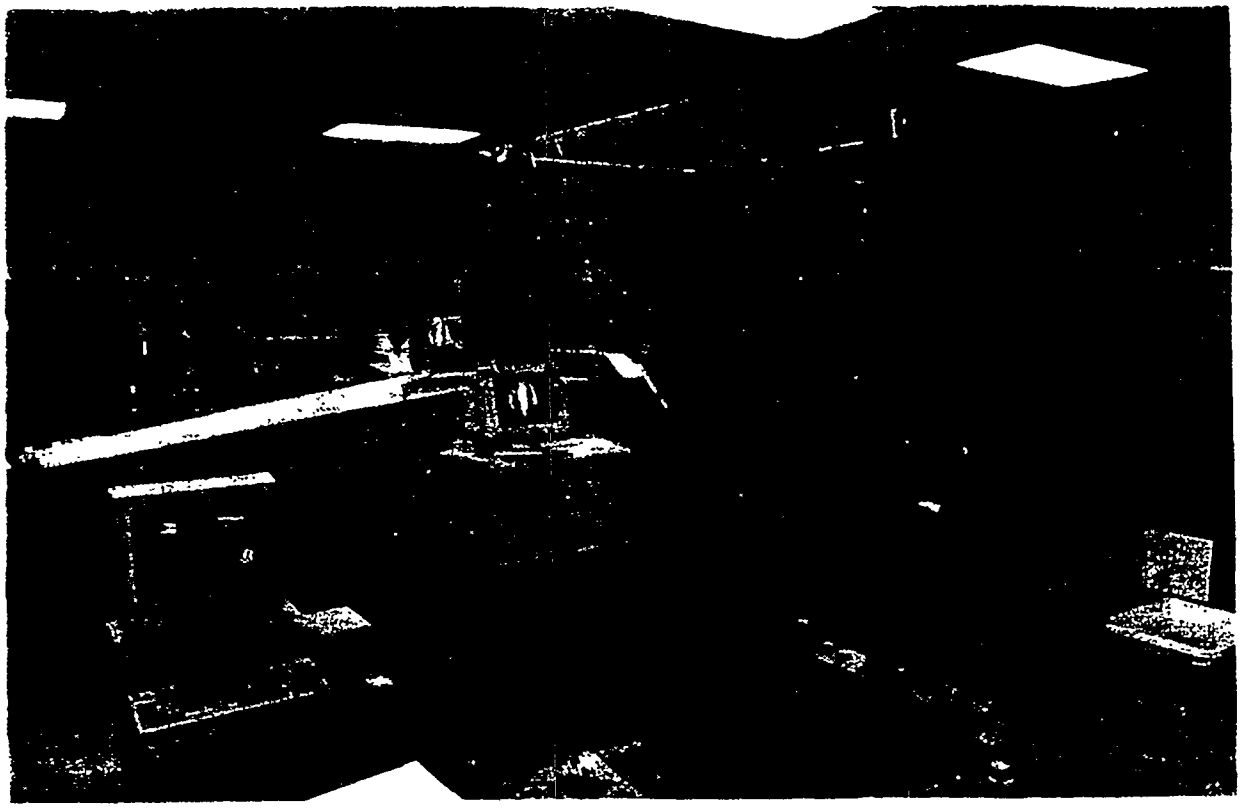

Figure 1b:
The GPIxp 102 / 457 mm (4"/18") interferometer (photos)

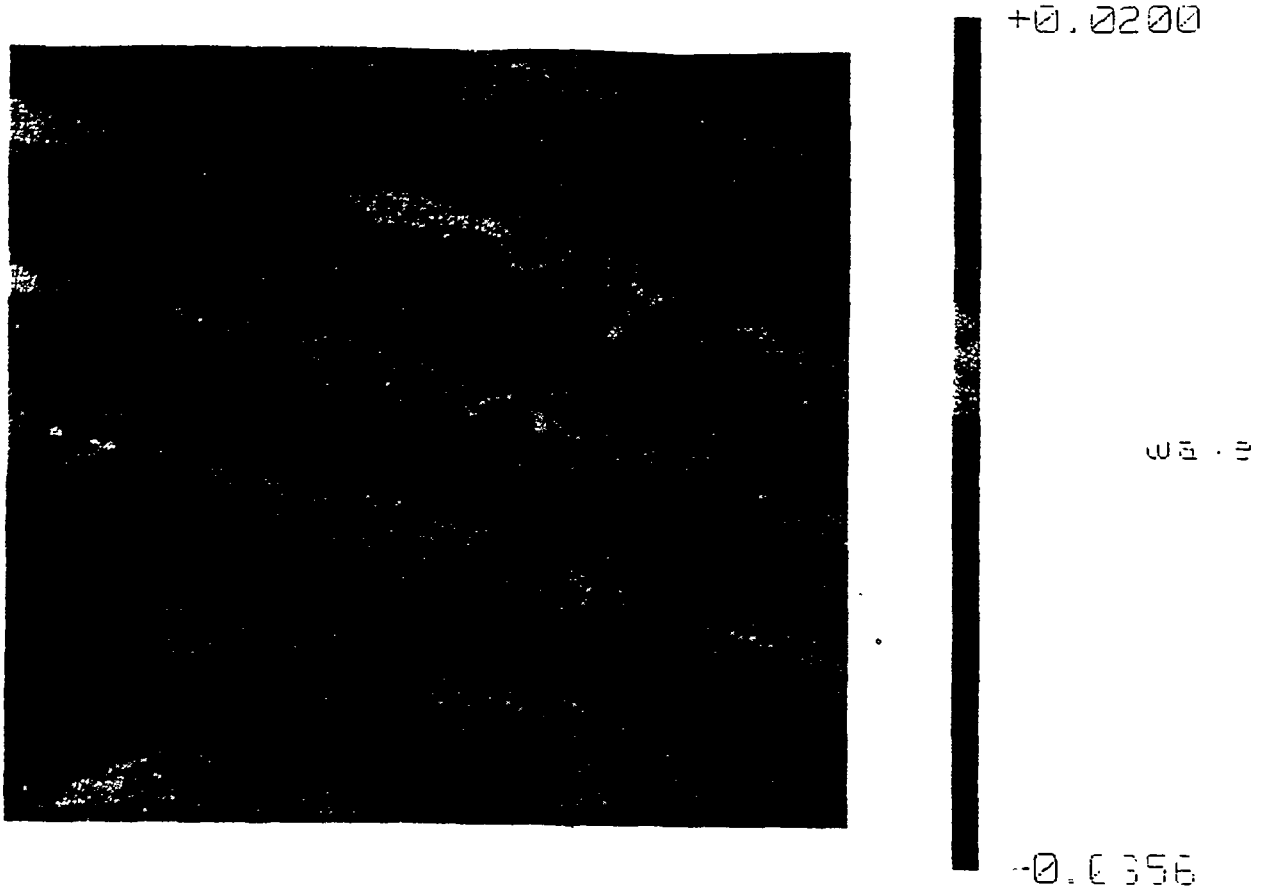

Figure 2:
A 38 mm square phase map of the reflected wavefront of crystal LL-8-2: P-V = 0.086 λ, @ 633 nm

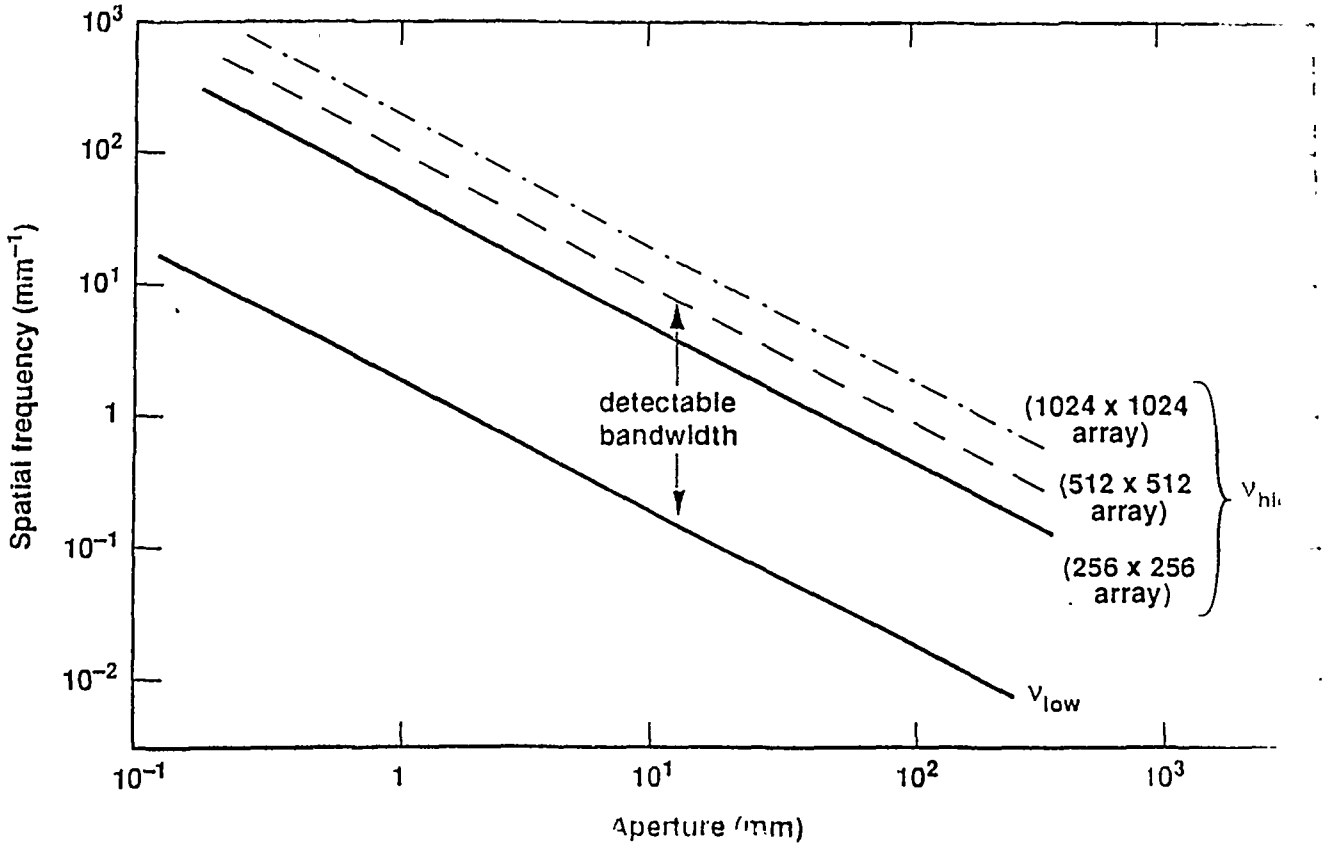

0-39-0094-3318

Figure 3:
Ideal, or detector limited, frequency bandwidth vs. aperture diameter and detector element count.

optical component: reason for concern - priority*	spatial wavelength measured, mm "roughness" < 0.12	"mid-spatial wavelengths" 0.12 - 33.0	"optical figure, curvature" > 33.0
laser slabs	energy loss -3	pin hole closure - 2 beam modulation, damage - 1	far-field modeling - 1
KDP crystals: Pockels cell	energy loss - 3	pin hole closure - 2 beam modulation, damage - 1	far-field modeling - 1
frequency conversion	energy loss - 3	beam modulation, damage - 1	beam modulation, damage - 1 conv. efficiency - 3
mirrors: cavity	energy loss - 3	pin hole closure - 1 beam modulation, damage - 1	far-field modeling - 1
transport/turning	energy loss - 3	beam modulation, damage - 1	far-field modeling - 1
polarizer	energy loss - 3	pin hole closure - 1 beam modulation, damage - 1	far-field modeling - 1
lenses: CSF	energy loss - 3	pin hole closure, energy loss - 2 beam modulation, damage - 1	far-field modeling - 1
TSF	energy loss - 3	beam modulation, damage - 1	far-field modeling - 1
Focus	energy loss - 3	beam modulation, damage - 1	energy loss - 3
windows: Pockels cell	energy loss - 3	pin hole closure - 2 energy loss - 2 beam modulation, damage - 2	far-field modeling - 1
gas box	energy loss - 3	beam modulation, damage - 2	far-field modeling - 1
debris shield	energy loss - 3	beam modulation, damage - 2	far-field modeling - 1
How measured ?			
interference microscope	40 x Fizeau	1x Fizeau	
phase shifting interferometer		10 - 100 mm aperture	100 - 457 mm aperture
static fringe interferometer			full aperture (813 mm)

* priority: 1 - highest, 3 lowest
shaded entries indicate measurements have been made

Figure 4:
Metrology matrix for NIF optical components

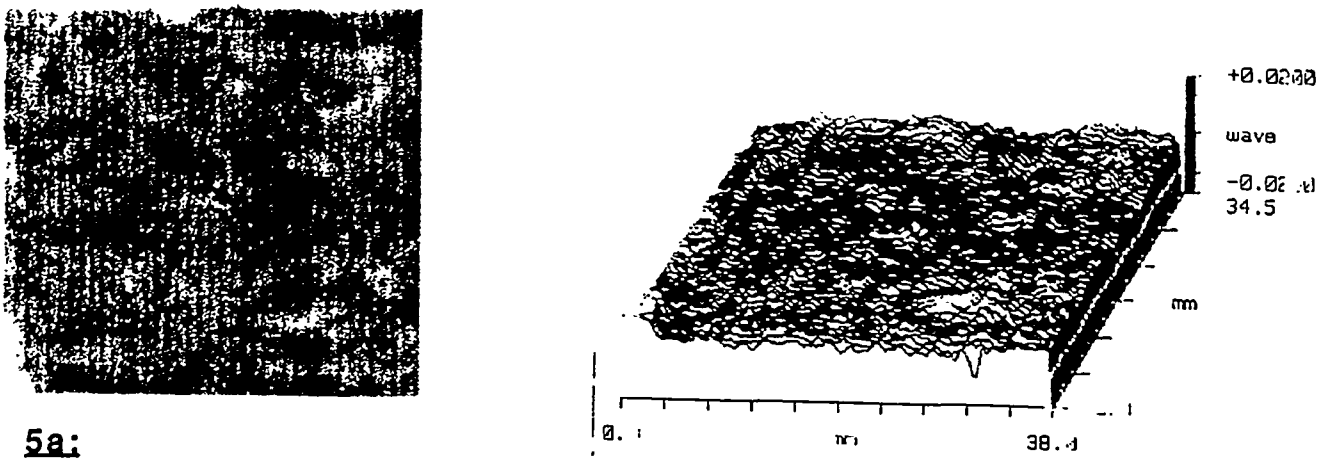

5a:
A relatively random, unmodulated wavefront, P-V = 0.19 λ, @ 633 nm

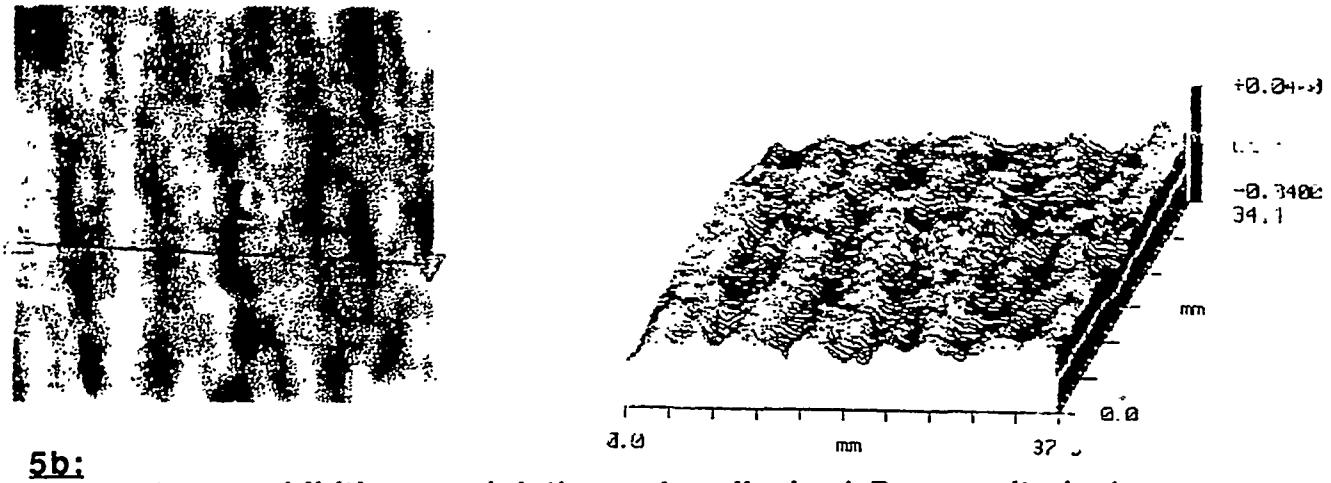

5b:
A wavefront exhibiting modulation primarily in 1-D, magnitude is λ/70 with a scale lengths from 5 - 7 mm, P-V = 0.35 λ, @ 633 nm

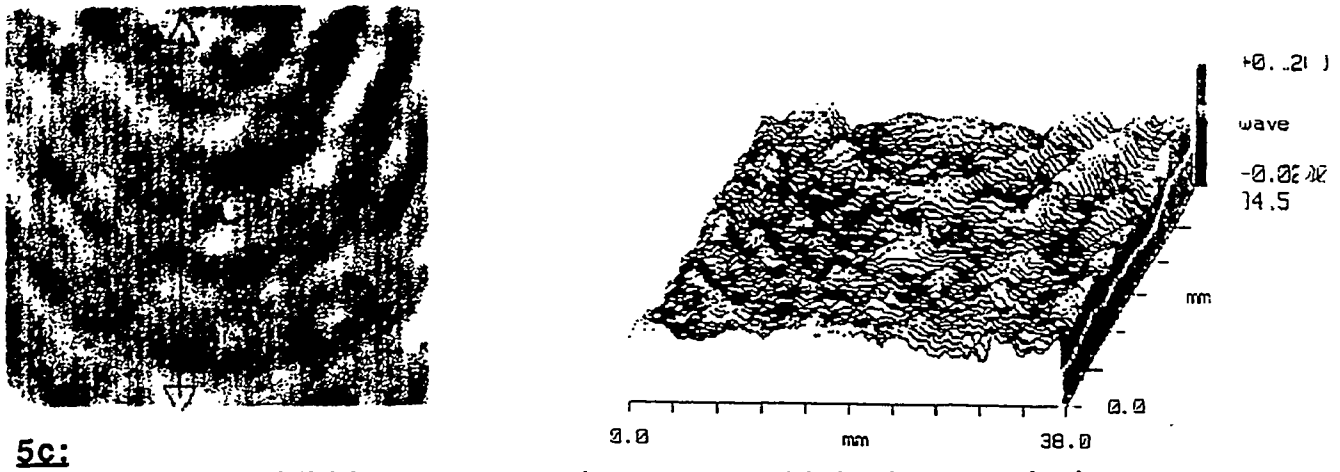

5c:
A wavefront exhibiting complex (curved, multiple frequencies) modulation, magnitude is λ/100 with scale lengths from 5 - 7 mm, P-V = 0.17 λ, @ 633 nm

Figure 5:
38 mm square aperture transmitted wavefronts from laser slabs

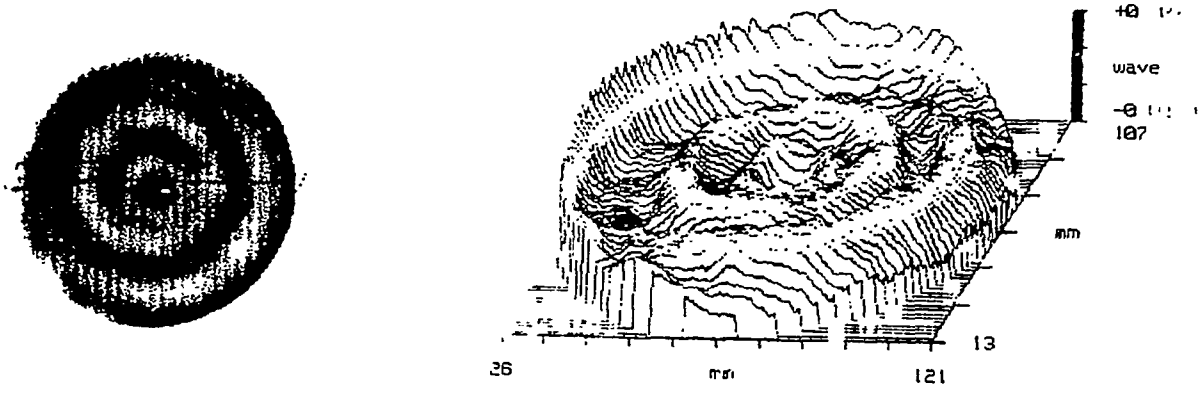

Figure 6:
Transmitted wavefront modulation detected in a spatial filter lens, P-V = 0.037 λ, @ 633 nm

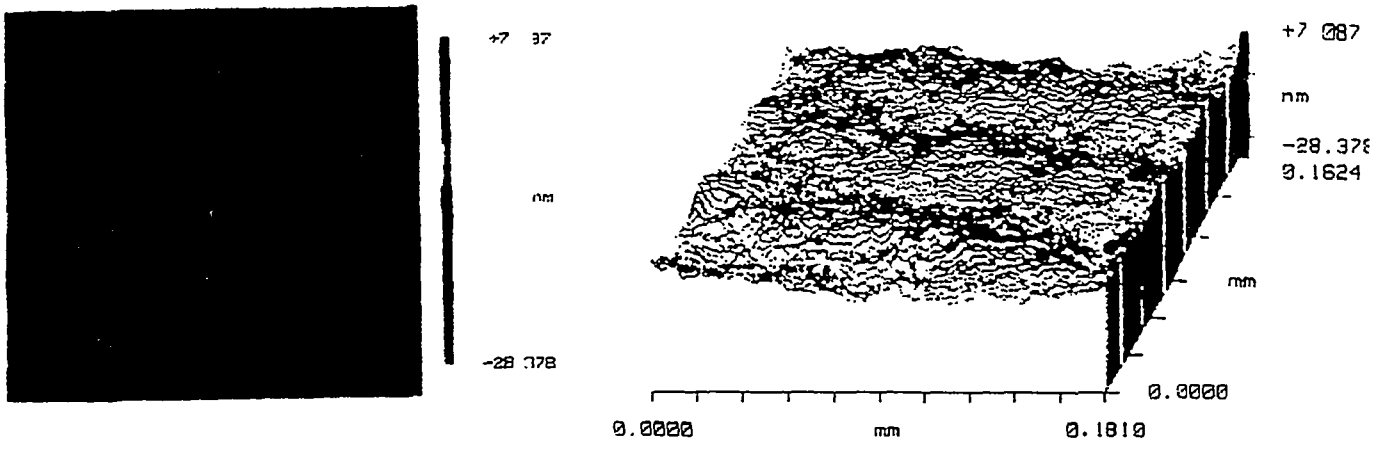

7a:
Surface #1 aspheric, magnitude of modulation 9.1 nm, over-all P-V = 35.5 nm

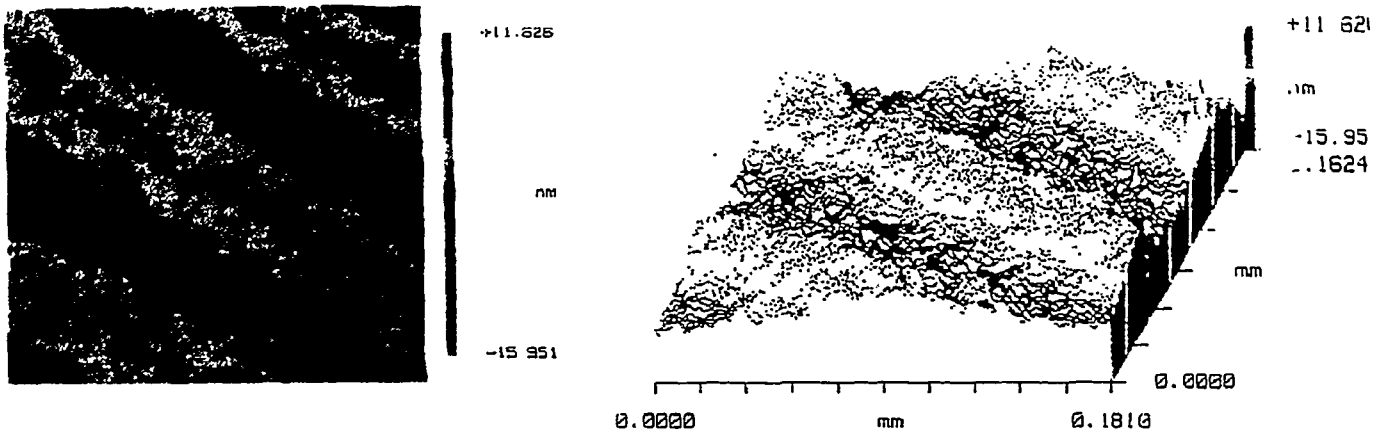

7b:
Surface #2 spherical, magnitude of modulation 10.6 nm, over-all P-V = 27.6 nm

Figure 7:
Short scale length surface features detected on both the spherical and aspheric surfaces of a spatial lens

8a:
Phase map with multiple profiles defined

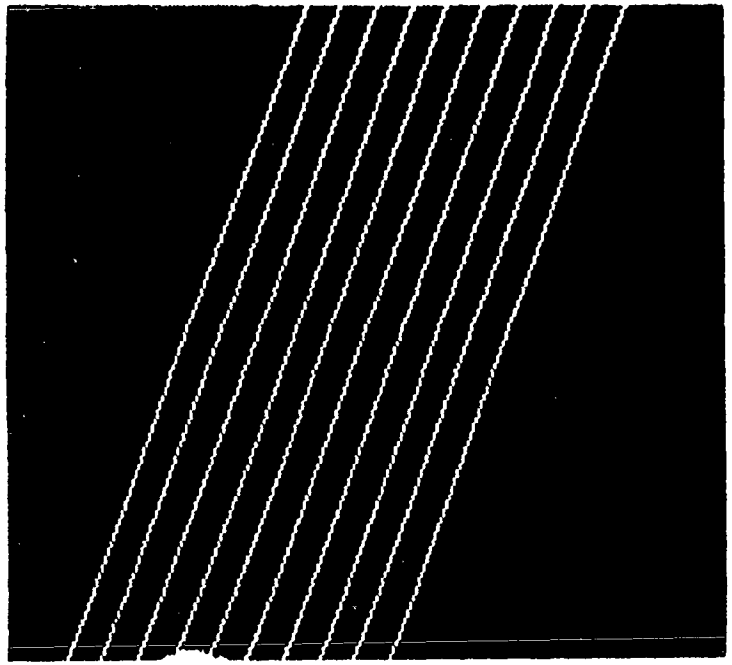

8b:
Profiles of phase height vs. position

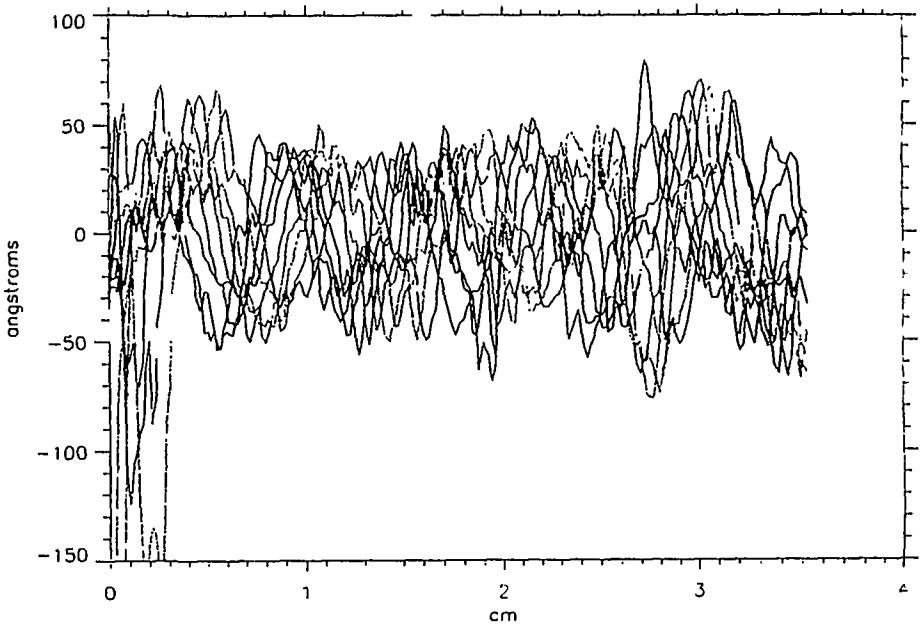

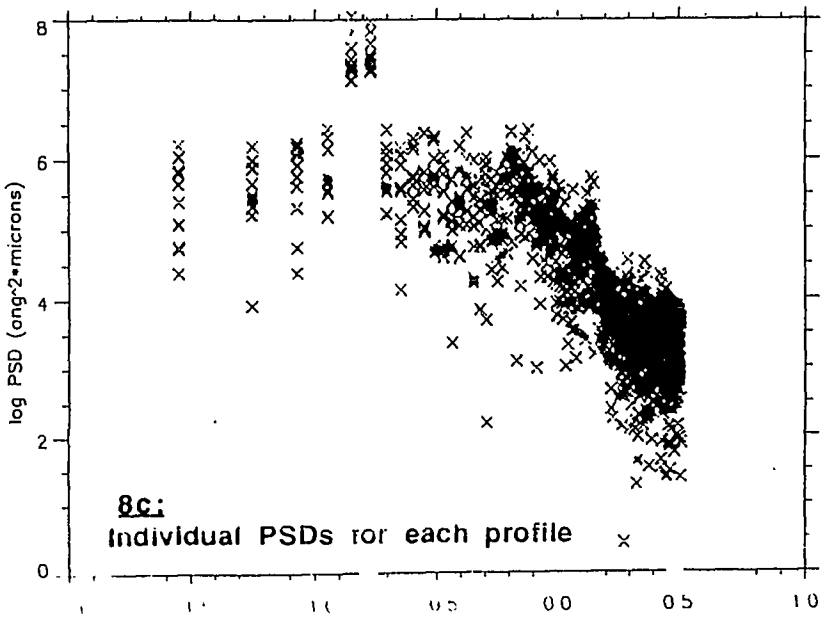

8c:
Individual PSDs for each profile

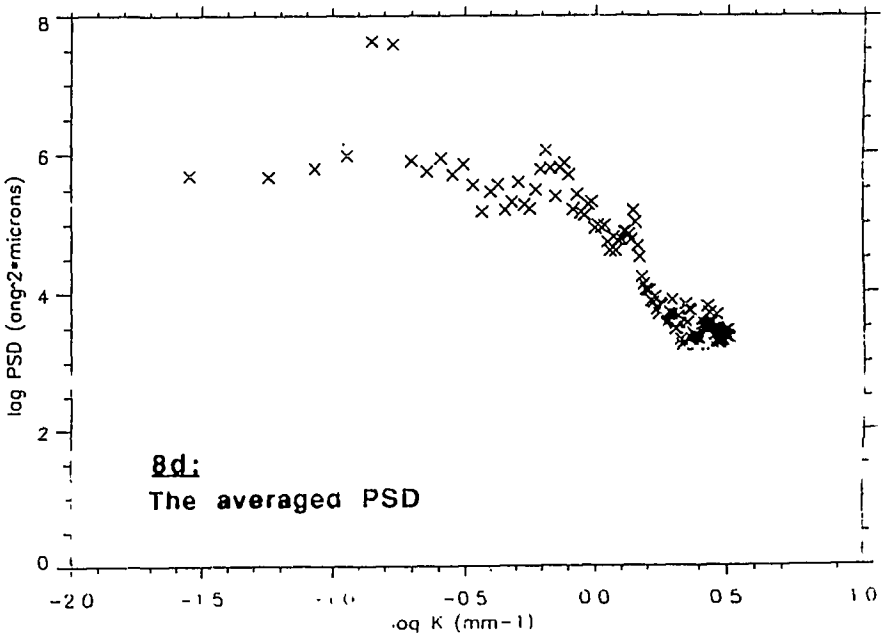

8d:
The averaged PSD

Figure 8.
An example of 1-D Fourier analysis of the reflected wavefront from a diamond turned KDP crystal surface (same data as Figure 2)

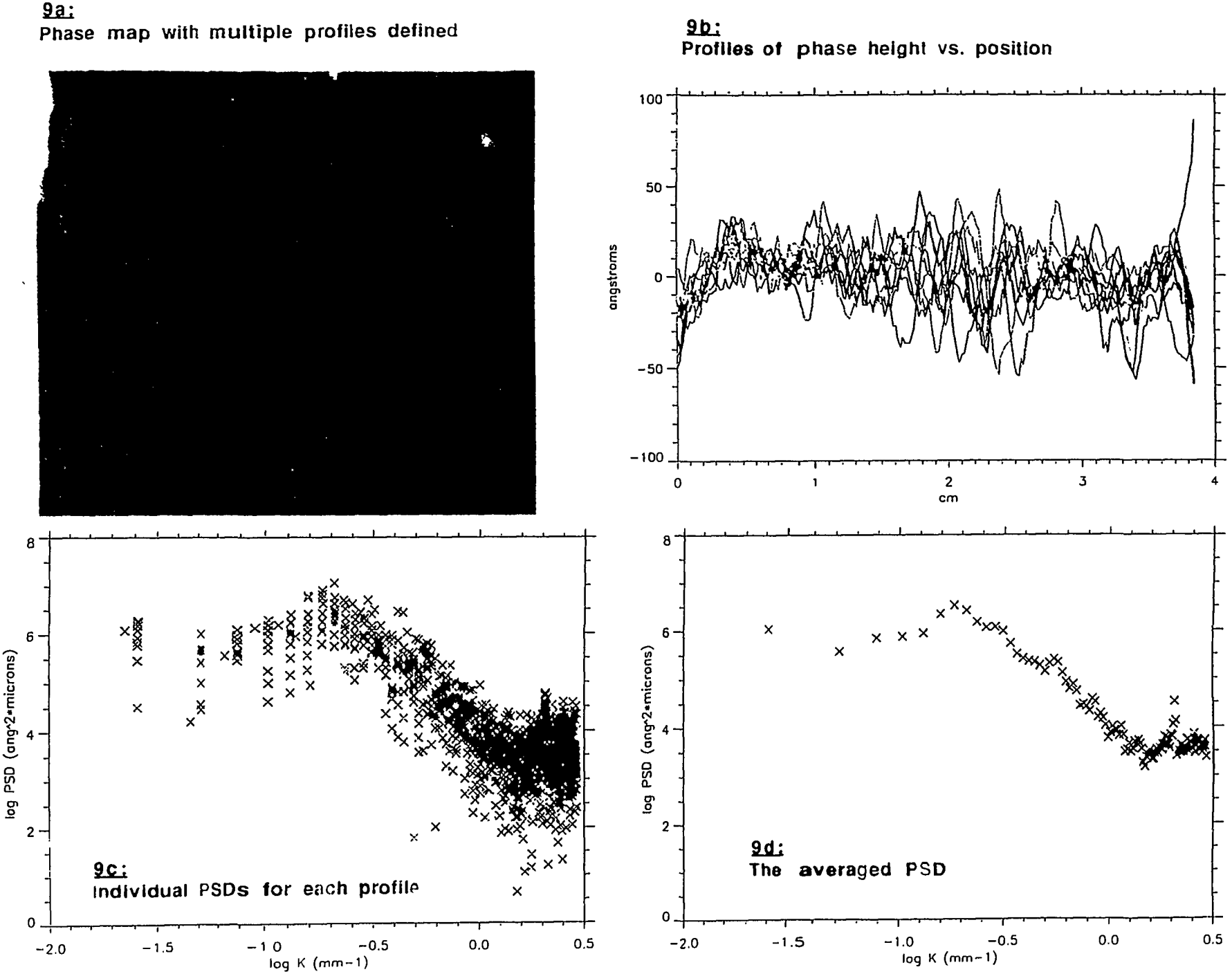

Figure 9:
Example of 1-D Fourier analysis of a transmitted wavefront

10a:
Phase map data

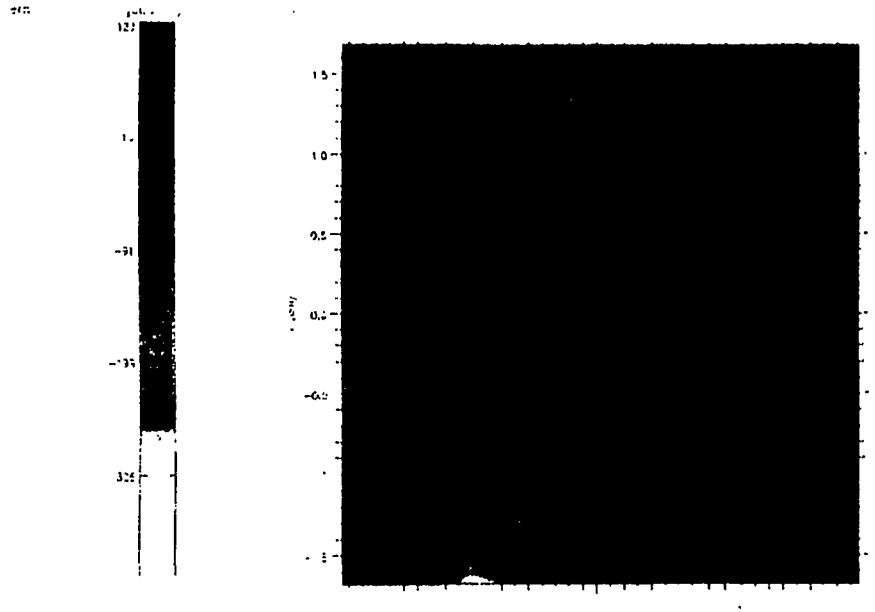

10b:
Phase map with Hanning window applied

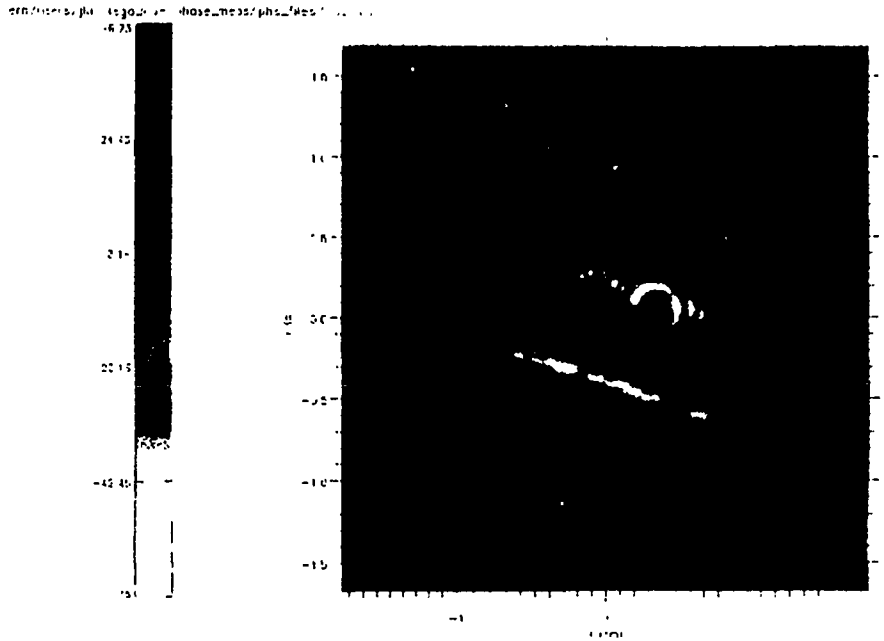

10c:
PSD calculated in 2-D

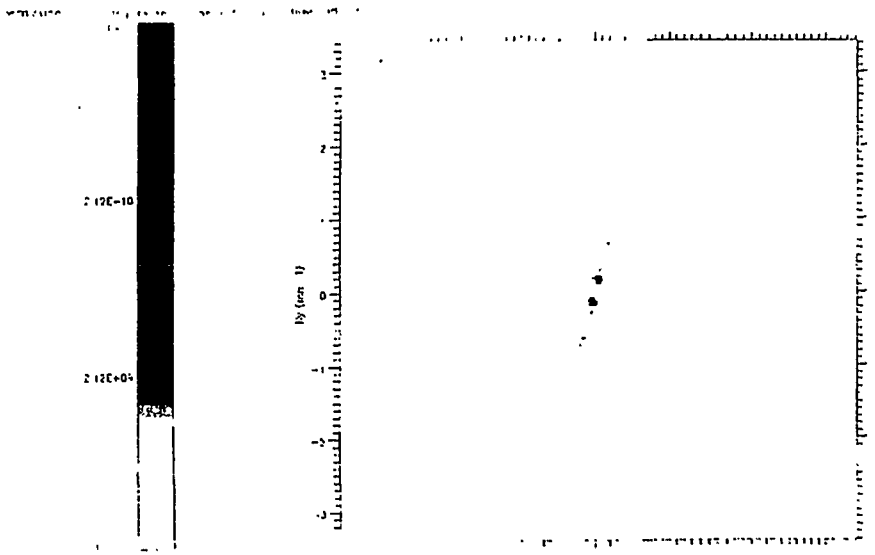

10d:
PSD surface

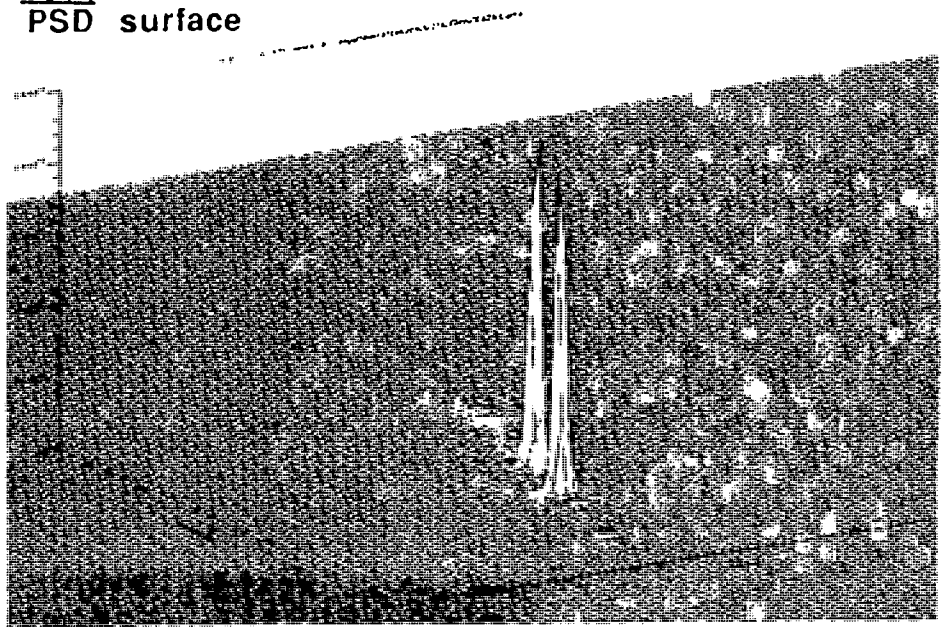

Figure 10:
Examples of 2-D Fourier analysis of a reflected wavefront (same data as Figures 2 and 8)

11a:
Phase map data

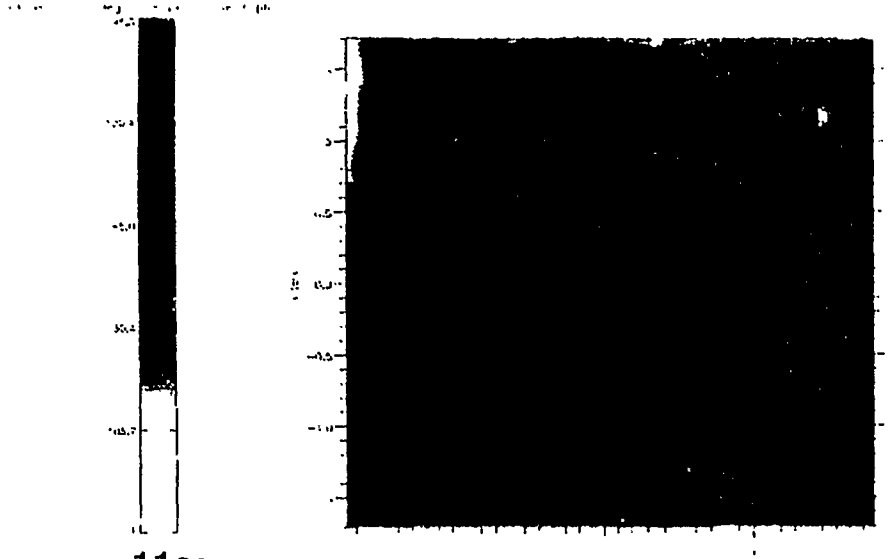

11b:
Phase map with Hanning window applied

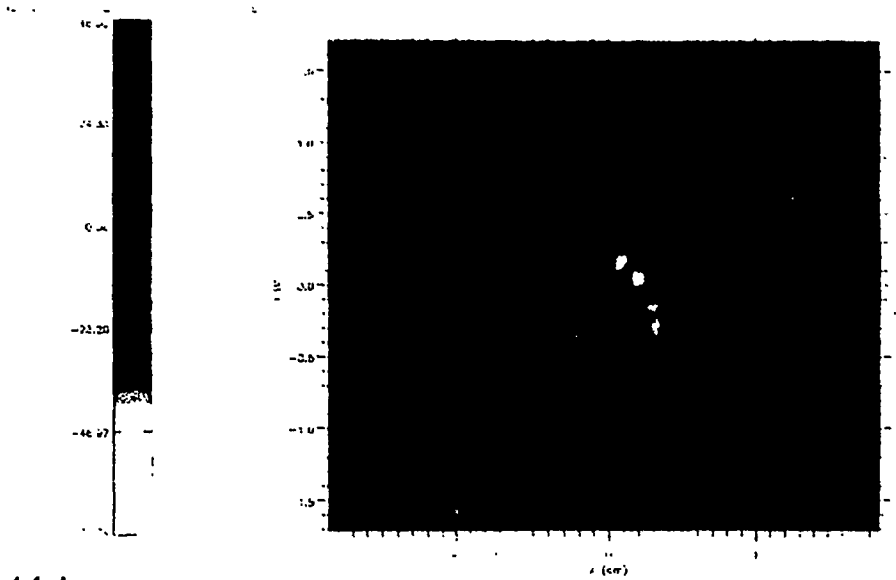

11c:
PSD calculated in 2-D

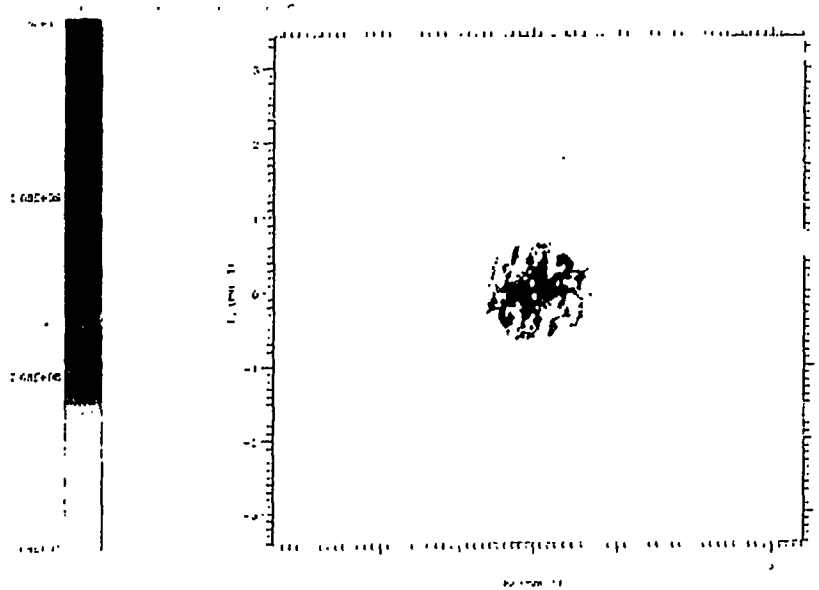

11d:
PSD surface

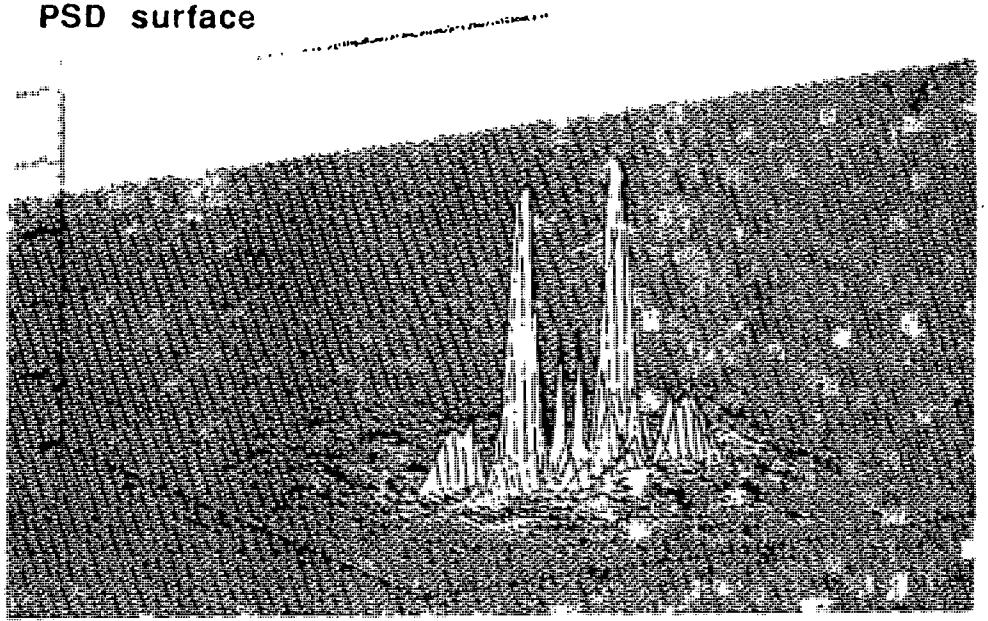

Figure 11:
Examples of 2-D Fourier analysis of a transmitted wavefront
(same data file as Figure 12)